Novelty Detection of Foreign Objects Using Grating-Based Interferometry

Monica J. Emerson

Kongens Lyngby 2014
IMM-M.Sc.-2014-

Technical University of Denmark
Department of Applied Mathematics and Computer Science
Matematiktorvet, building 303B,
2800 Kongens Lyngby, Denmark
Phone +45 4525 3351
compute@compute.dtu.dk
www.compute.dtu.dk IMM-M.Sc.-2014-

Summary (English)

Quality assurance in food industries is essential, both in regards to consumer satisfaction and also food safety. During food processing, unwanted foreign objects can be introduced to food products, which can both be unappetizing and hazardous for the consumer. Nowadays, X-ray conveyor belt solutions can detect non-organic materials, but finding organic foreign objects in food with typical X-ray systems is not a simple task.

The goal of the thesis is to demonstrate the improvement introduced in foreign body detection by a new X-ray imaging technique when organic materials are potential foreign bodies. This novel X-ray technique is based on interferometry, created by adding gratings to a conventional X-ray source. This technique provides information about a sample's absorption, refraction and scattering properties; whereas conventional X-rays just grant the absorption profile of a sample.

A grating-based interferometer set-up is available at *Technische Universität München*, where data was acquired personally. Each image, consisting of three imaging modalities (absorption, phase contrast and dark-field), contains a food sample contaminated by different sized foreign bodies (organic and non organic). Several food products were imaged. These products have different properties and are of importance to the **NEXIM** project (New X-ray Imaging Modalities for safe and high quality food) collaborators.

In this thesis, the performance of two classification algorithms is compared, one is supervised and the other is unsupervised. Focusing on the unsupervised technique, food models with varying number of features are compared and detection results are contrasted with those obtained when using only the absorption.

Preface

This M.Sc. thesis was carried out at the Department of Applied Mathematics and Computer Science of the Technical University of Denmark in fulfilment of the requirements for acquiring *Ingeniería Superior de Telecomunicaciones, esp. Comunicaciones* at *Universidad de Zaragoza*.

The project was supervised by Line Clemmensen and Hildur Einarsdottir, both within the DTU Compute department. The M.Sc. thesis period was 20th of January 2014 to 10th June 2014.

The project is credited with 30 ECTS points and is concerned with the detection of foreign objects in food, making use of a novel X-ray technique.

Lyngby, 10-June-2014

Monica J. Emerson

Acknowledgements

I would like to thank both of my supervisors, Line and Hildur. Without Line, the opportunity to perform this thesis would not have been possible. Moreover, Hildur played an essential role throughout the thesis; providing her knowledge and advice, as well as enabling the data collection at *Technische Universität München* (TUM). This allowed me to travel personally to Munich where I could work with the X-ray set-up. In addition, I acknowledge the partners involved in the **NEXIM** project (New X-ray Imaging Modalities for safe and high quality food), for financially supporting my trip to Munich.

I would like to thank the members of the image analysis group at DTU Compute for their valuable feedback while the project was being undertaken and, in general, everyone in the Data Analysis and Statistics Area for making me feel welcome. Specially to Ruta, who lent me her desk, Merete, who made some very nice comments on my work, and David, such a lovely person that will make you smile in your bad moments.

I would like to express my gratitude to the people in the Physics department at TUM. Not only the set-up had to be booked by Kai Scherer, but also Konstantin Böll was attending and helping out while using the set-up.

Last but not least, this thesis would not have been possible without the financial support of my parents. My dad, Rupert, was also the key proofreader of the thesis and such a good listener and advisor towards my career, demonstrating his great consultancy abilities. Thanks to my sister, Becky, and my mum, María Ángeles, for proofreading the final version. And specially to my mum, for dedicating her whole life to her daughters.

Abbreviations

BIF	Basic Image Features
CM	Confusion Matrix
EM	Expectation-Maximization algorithm
FS	Feature Selection
FP	False Positives
FPR	False Positive Rate
GBI	Grating-Based Interferometry
GPU	Graphic Processing Unit
GMM	Gaussian Mixture Model
ROC	Receiver Operating Characteristic
SVM	Support Vector Machines
TP	True Positives
TPR	True Positive Rate
TUM	*Technische Universität München*

Contents

Chapter 1

Introduction

This chapter first explains the motivation for the detection of foreign bodies and then explains the challenge that organic materials represent. After introducing the background for this new X-ray imaging technique, the state of the art on foreign object detection is discussed.

1.1 Motivation

The detection of foreign objects plays an important part in the quality assurance of food. It is never appealing to find a spider or a stone in your food, nor hygienic. Getting injured while eating could be a very negative advertisement for a food manufacturer, which could even result in legal action. For this reason, quality assurance is a high priority task for food producers.

This project will provide an answer to two major questions:

1. How can this inspection be performed in an automatic and efficient manner?
2. Can we find organic materials - such as insects, plastics or wood - using X-rays?

1.2 Problem Formulation

In countless fields there is a need for obtaining internal structural information on complex objects without an actual dissection. Additionally, obtaining such information can be achieved with X-ray imaging, where the sample can be probed in a non-invasive manner. This structural information is of use in a wide variety of industries for inspection purposes, including food, construction and pharmaceutical product quality assurance, airport security and medical diagnostics, among others.

Typical X-ray systems have been used for many years for in-line detection of foreign bodies in food products. Nevertheless, conventional X-ray absorption contrast is not suitable for detecting differences between different soft materials, which seem much more challenging. However, improved contrast in imaging soft matter can be encountered via the use of X-ray imaging methods based on the sample's refraction and scattering properties. This drastically increases the number of scenarios where the object's structural information can be obtained, boosting the number of possible applications.

The aim of this study is to detect foreign objects - objects that are not supposed to be in a specific place - namely in food products, using a novel technique known as Grating-Based Interferometry (GBI). With this technique, a multimodal image consisting of three modalities (transmission, phase contrast and dark-field) is available for all kinds of food samples.

For the purpose of investigating the applicability of using the GBI technique to detect foreign objects in food, several food products should be chosen together with a range of foreign objects which are typically found in the industry.

Figure 1.1 gives an overview of suggestions given by industrial collaborators on foreign bodies (contaminants) and size ranges which are commonly encountered in certain food products.

Food Product	Industrial Partner	Contaminant	Size distribution
Minced meat	Danish Crown	Bone Plastic Cartilage	0.5 mm, 1 mm, 5 mm, 10 mm, 50 mm, 100 mm, 1 cm, 5 cm, 10 cm
Bread	Lantmannen Schulstad Kohberg	Stones	?
Milk products	Arla	?	?
Chicken products	Lantmännen Danpo	Bone Cartilage Plastic	0.5 mm, 1 mm, 5 mm, 10 mm, 50 mm, 100 mm, 1 cm, 5 cm, 10 cm
Pet Food	Arovit Petfood	?	?
Spring rolls	Daloon	String Stones	?

Figure 1.1: Proposed food products, foreign bodies and their sizes by industrial collaborators.

In Figure 1.2 the different materials used as foreign bodies can be observed in a specific food product, rye bread.

Figure 1.2: *Purple*: Soft plastic, *Pink*: Hard plastic, *Blue*: Glass, *Green*: Wood, *Red*: Insect, *Orange*: Metal, *Cyan*: Stone and *Yellow*: Rubber.

By virtue of this new imaging technique, the refraction and scattering properties are taken into account, as well as the sample's absorption. As a result, soft matter may be found in higher contrast, whereas it was not highlighted by conventional X-ray.

In Figure 1.3 we can see that different materials stand out best in different modalities. Glass, metal and stones can be detected easily by the difference in intensity from the absorption modality (transmission). On the contrary, soft and hard plastic, rubber, insects and wood are better enhanced in the other two modalities.

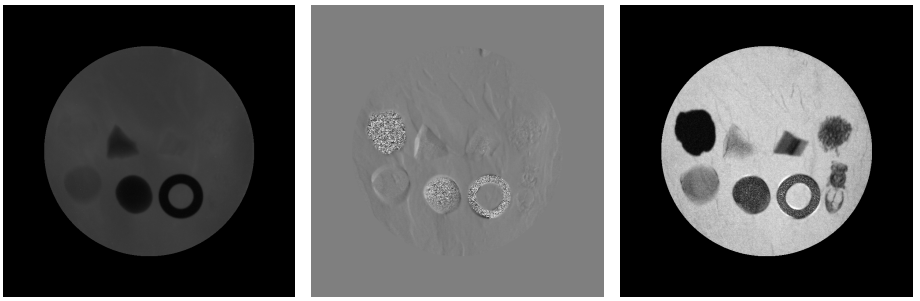

(a) Absorption (b) Phase contrast (c) Dark-field

Figure 1.3: Rump steak with foreign bodies shown for all three GBI modalities. Foreign bodies are seen with varying contrast between the different modalities.

Summarizing, in order to reach the target of detecting foreign objects in food products, a test case will be set up. For this test case, several steps are needed.

1. The data needs to be collected, so the food products and foreign objects that are going to be investigated have to be identified, as well as limited so that the data acquisition is reasonable.
2. In order to analyse the acquired data, two different algorithms will be probed and different parameters will be optimized.
3. These algorithms' performance will be compared, and results will be displayed.
4. The gain in efficiency, thanks to these new X-ray modalities, will be presented, compared to the efficiency in detection that conventional X-ray provided.

Before going into more details of the specific case study of this project, the background literature, and state of the art will be discussed.

1.3 Literature Study

Imaging techniques have been essential in a wide range of areas. In fact, when a new imaging technique was invented, it was usually followed by a scientific implementation. This development can be observed after the discovery of X-rays by Wilhelm Röntgen in 1895 [Röntgen, 1895], when X-rays were used for clinical purpose [Spiegel, 1995]. A similar evolution can be noted in optical microscopy. Imaging of biological samples was carried out after the invention of the first microscope in the 17th century [Hooke, 1665].

During the 20th century, new forms of imaging appeared, such as dark-field and phase contrast imaging [Rost and Oldfield, 2000, Zernike, 1942]. Instead of relying on absorption-based contrast - like microscopy - they measure refraction and scattering, respectively.

In the last decade, there has been an enormous evolution in X-ray imaging, involving the use of X-ray techniques which are based on these modalities, phase contrast and dark-field. These modalities are more sensitive than absorption to low impedance materials, such as organic materials. Grating-based interferometry allows us to obtain the three modalities simultaneously with pixel correspondence (absorption, phase contrast and dark-field), can be implemented in laboratories [F. Pfeiffer and David, 2006] and shows potential towards industrial implementation [Kottler et al., 2010].

Several studies have been carried out concerning this recent imaging technique, its parameters and applications [Nielsen, 2012, Bech, 2009]. Other strategies, which do not make use of dark-field and phase contrast, have been discussed when it comes to organic foreign object detection, such as increasing absorption contrast applying low X-ray energies in the 10-25 keV range, in order to benefit from the higher attenuation of light elements [M. S. Nielsen and Fidenhans, 2012], but concluded that grating-based imaging (GBI) was an option worth looking into, as it does not imply a lower scanning speed, nor such high X-ray power levels.

1.3.1 How do X-rays find foreign objects?

1.3.1.1 What are X-rays?

X-Rays refer to an invisible form of electromagnetic radiation, of the same nature as radio waves, microwaves, infra-red and visible light, ultraviolet and Gamma rays. The main difference between X-rays and Gamma rays is the origin: X-rays are formed by extra-nuclear events, whereas Gamma rays have a nuclear origin. The energy of the X-rays is, in general, in between the ultra-violet radiation and the natural Gamma rays' energy, as we can see in Figure 1.4.

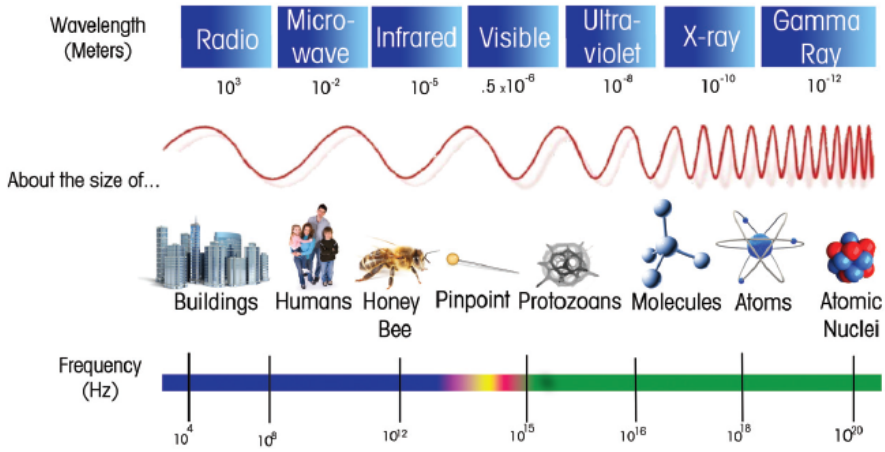

Figure 1.4: Electromagnetic Spectrum.

The fact that X-rays do not pass as easily through all materials, creates this difference in intensity which can be observed in the absorption contrast. This ability to penetrate a material is also dependent on the material's density and thickness. As can be seen in Figure1.5, the thicker the cheese is, that is to say, the more layers stacked, the harder it is for the rays to cross the material. As a result, less amount of signal will reach the detector, which implies a darker intensity. The foreign bodies that are denser than cheese stand out in this modality.

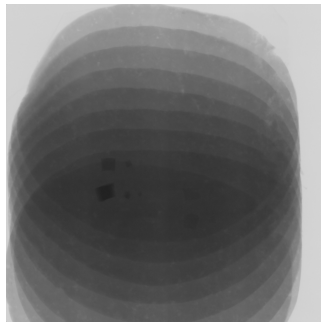

Figure 1.5: Absorption modality for stacked slices of cheese with several foreign bodies.

1.3.1.2 Different approaches to scanning for foreign bodies

It should be noted that machine and human vision, both relying on images, are very different. For this reason, it is difficult, but necessary, to prevent our own preconceptions from influencing the type of image processing that should be applied.

Some studies have tried to find foreign bodies within an absorption image [B. G. Batchelor and Graves, 2004]. The techniques rely on the difference between intensity, that is, between density of the foreign objects and the specific food product. These intensities are homogeneous for some food products and foreign bodies, or can follow a certain pattern. For example, a certain arrangement can be observed in minced meat, Figure 1.6. For this reason, studies referring to texture analysis are also of importance. Moreover, shapes could also be analysed, but in this case they are not useful, as fragmented objects could have infinite different shapes.

This thesis work focuses on combining the GBI technique with data analysis relying on statistical, image analysis and machine learning techniques. Both spectral (intensity) and spatial (texture) information are considered particularly relevant.

1.4 Outline

The outline of the remainder of the thesis is the following:

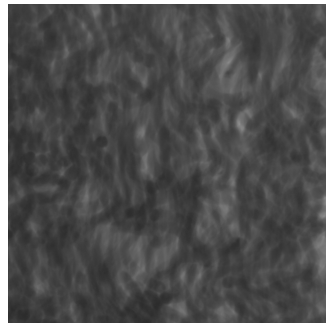

Figure 1.6: Absorption image of minced beef without foreign bodies.

1. In chapter 2, the focus is the design facet. First, a quick description of the used X-ray set-up for the data acquisition. Second, a discussion of the reasons for choosing the different materials (food and foreign bodies). And third, an introduction of the implemented methods, followed by a brief understanding of each of the used methods and the motivation towards their selection.

2. In chapter 3, the obtained results are presented. First, different Gaussian models are compared for one single product. Second, the performance of the Gaussian model is compared to Support Vector Machines for one specific set of features. Finally, several food products are probed.

3. In chapter 4, conclusions concerning the results are drawn and possible future work is discussed.

Chapter 2

Design

The following chapter looks at the design aspect of the novelty detection task. The grating-based imaging and the detection methods used throughout the report are presented and discussed.

2.1 Set-up

In typical X-ray imaging the change in beam amplitude is measured to calculate a sample's absorption properties. This is portrayed in Figure 2.1, where the green beam profile shows a decrease in amplitude when travelling through an absorptive material. For grating-based imaging, the set-up is expanded to include gratings, which create an interference pattern. In addition to the absorption, the sample's refraction and scattering can be calculated by analysing this interference pattern. These refraction and scattering properties are observed in the detector as a beam shift and broadening, respectively. The blue and red beam profiles in Figure 2.1 illustrate this.

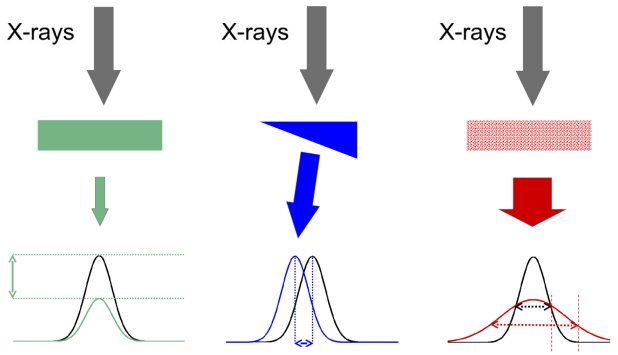

Figure 2.1: Interactions: The change on an incoming beam by inserting a material, which is *Green*: absorptive, *Blue*: refractive or *Red*: ordered in its micro-structure [Nielsen, 2012].

In Figure 2.2 the GBI experimental set-up is illustrated. Grating G1 produces an interference pattern of periodic fringes, which are transversal to the beam direction. The change in position and amplitude of the fringes is investigated with a second grating G2 part by part (accomplished by stepping one of the gratings, G1 in this specific set-up), obtaining measures for the sample's absorption, refraction and scattering properties simultaneously. The third grating G0 adds spatial coherence to the X-ray beam [Nielsen, 2012, Bech, 2009].

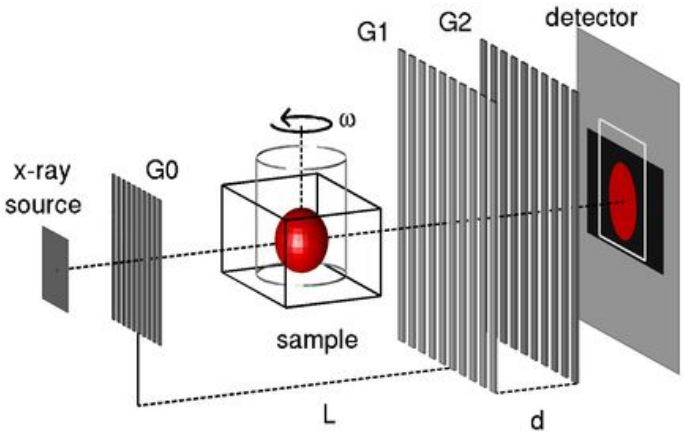

Figure 2.2: Sketch of a Talbot-Lau interferometer [Bech, 2009]

The grating-based X-ray system which has been used for imaging the food samples is located at the Chair of Biomedical Physics of the *Technische Universität München* (TUM). It is a three grating Talbot-Lau interferometer, consisting of a conventional X-ray tube, a source grating, a phase grating and an analyser grating. The gratings were produced by Microworks (Karlsruhe, Germany) with grating periods of 10 μm, 3.24 μm and 4.8 μm. The phase grating introduces a phase-shift of $\pi/2$ to incoming X-rays with an energy of 27 keV. The distance between the source and phase grating is 106 cm, whereas the distance between the phase and analyser grating is 51 cm. For more information see [Scherer et al., 2014]. A photo of the set-up can be seen in Figure 2.3.

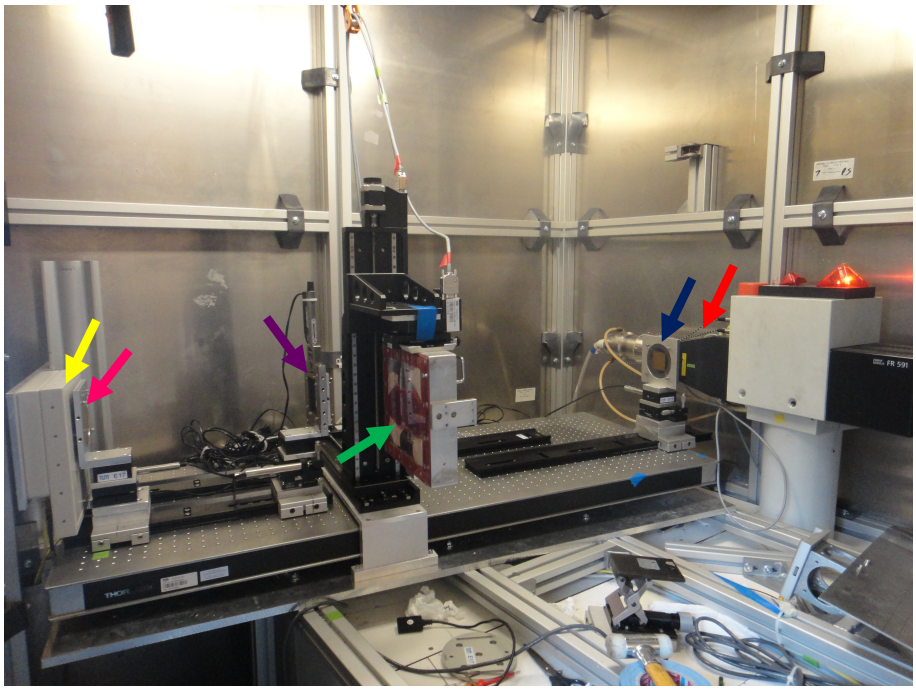

Figure 2.3: Photo of set-up at *Technische Universität München* (TUM). *Red*: X-Ray source, *Blue*: Grating G0, *Green*: Sample holder, *Purple*: Grating G1, *Pink*: Grating G2 and *Yellow*: Sensor/detector.

The set-up had been optimized for breast tissue, which is similar in attenuation to food products. The parameters of the set-up were not changed in order to avoid an extensive optimization study. Ideally, it should have been optimized for each of the seven food products which were imaged.

The effective energy was set to 25 keV and each sample was imaged from one single projection and the grating was stepped 9 times.

The integration time, t_{int}, was the only parameter which was changed while imaging. Most of the time it was set to two seconds, but for two of the images (turkey and steak with 4x4x4 mm foreign bodies) it was set to one second. It can be seen in Figure 2.4 that when the integration time is too low, 0.2 seconds, there is a lot of noise in the image. In contrast, the higher that t_{int} is, the more artefacts can be appreciated, such as phase wrapping, as can be seen when t_{int} is two seconds. As a trade-off value, the exposure time was chosen to be one second for this particular image. But, in general, two seconds seemed a good adjustment for the exposure time, so that the images did not include too much noise or artefacts.

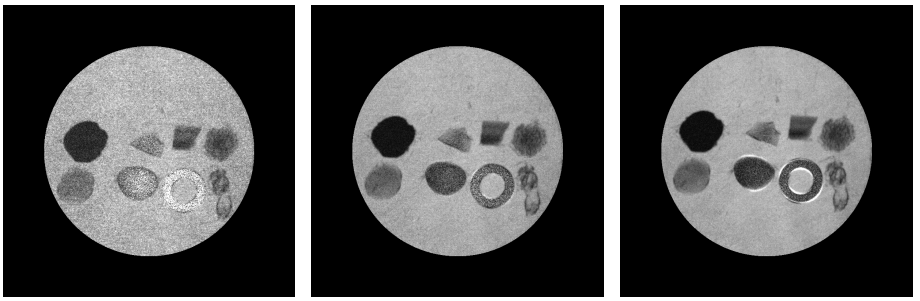

(a) $t_{int} = 0.2$ (b) $t_{int} = 1$ (c) $t_{int} = 2$

Figure 2.4: Turkey imaged with varying integration times.

2.2 Materials

The data consists of three imaging modalities, where food containing foreign bodies is imaged. This data was acquired personally at the *Technische Universität München*.

Data acquisition is a slow process, both due to the fact that samples need to be manually placed in a sample container, set into the X-ray set-up, and that during the image acquisition the physical stepping of the grating is slow. For this reason, the option of synthesising data was considered. Unfortunately, it is not possible to synthesise data because the scattering of the different materials cannot be predicted. That is to say, the size of the foreign bodies in the dark-field modality can not be predicted, as it could be different depending on the

placement of the foreign body or on the specific type of wood, for example.

2.2.1 Food

To replicate the variation of food products within the food industry, a range of products differing in homogeneity has been chosen. Sliced cheese represents a completely homogeneous product whilst rye bread with seeds/kernels represents a non-homogeneous product. It is expected that the modelling of homogeneous products will be simpler.

In addition, the products have been selected to have different scattering properties, in order to cover varying differences in contrast between foreign bodies and food. Wheat bread contains flour, which is highly scattering due to its fine micro-structure. As a consequence, it is expected that foreign objects will not stand out in contrast very well in the dark-field modality of wheat bread, whereas the foreign bodies will be better appreciated in rye bread, as can be seen in Figure 2.5. In other words, when the scattering properties of food and foreign bodies differ more, the foreign bodies become more identifiable.

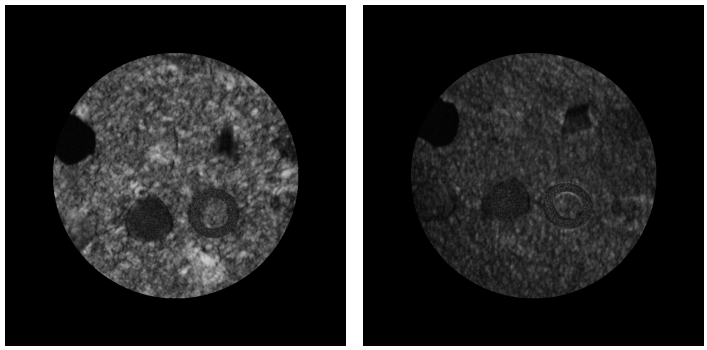

(a) Rye bread dark-field (b) Wheat bread dark-field

Figure 2.5: Different intensity contrasts in dark-field.

Moreover, as this thesis is a part of the NEXIM project[1], some of the chosen food products are those produced by the industries which collaborate in this survey. Minced meat, dairy products, bread and chicken are products of interest for our industrial collaborators.

[1] http://nexim.nbi.ku.dk/

Finally, the selected food products for imaging were minced meat, wheat and rye bread, turkey (similar to chicken), cheese, rump steak and salami. All food products were modelled, but only some are going to be highlighted in this thesis. Turkey and steak are similar, so only turkey will be considered. Salami and minced meat both contain meat and fat, so salami is the product which will be explored in greater depth. Regarding the bread, the focus will be on rye bread, as it is much more important for the Danish food industry. In fact, this new technique is not worthwhile for imaging wheat bread, due to its strong scattering properties. Furthermore, rye bread is particularly interesting as it is the least homogeneous product in texture.

2.2.2 Foreign Bodies

Foreign bodies are selected to have different absorption, refraction and scattering properties. In addition, foreign bodies proposed by NEXIM's industrial collaborators (see section 1.2) are also taken into consideration, as well as the data from a Japanese Survey.

Figure 2.6 shows the results from a Japanese survey on consumer contaminant complaints. It presents the frequency of encountering a certain contaminant, given the food is contaminated, and the level of difficulty when detecting these contaminants with normal X-rays. Typical X-ray techniques measure the absorption properties of the material, which means that the object will be more difficult to find the closer its density is to the food's density, i.e. closer to water's (1,000.00 kg/m^3). For this reason, paper and other organic materials are particularly hard to identify.

Contaminant	Percentage [%]	Difficulty detecting by X-ray	Contaminant	Percentage [%]	Difficulty detecting by X-ray
Insects	24.5	Difficult	Stone and sand	3.0	Easy
Bone (calcified only)	15.2	Medium	Paper, threads etc.	2.1	Difficult
Unclear	14.1	N/A	Vinyl	2.0	Difficult
Metal piece	7.3	Easy	Fly	1.8	Difficult
Hairs	6.6	Difficult	Wood chips	1.5	Difficult
Needles, wires etc.	6.5	Easy	Blade chips	1.2	Medium
Plastic and rubber	5.3	Medium	Staples	1.0	Easy
Glass fragments	3.9	Medium	Rat excrement	0.9	Difficult
Cockroach	3.1	Difficult			

Figure 2.6: Japanese survey results for consumer contaminant complaints [Takashi, 2009].

Finally, two major types of foreign bodies are selected:

1. Easy to find with absorption modality, such as metal, stone or glass.
2. Not visible in absorption modality, such as organic materials. Specifically, insects, wood, rubber and two types of plastic (hard and soft) are chosen.

In Figure 2.7 the chosen foreign bodies are illustrated. The sizes are selected approximately from 2x2x2 to 4x4x4 mm, as smaller objects are considered not to be harmful. The approximate thickness sizes measured in the direction of which the X-rays transverse through the objects are shown in Table 2.1.

Figure 2.7: Selected foreign bodies, with approximate sizes of 2x2x2, 3x3x3 and 4x4x4 mm, from left to right.

Type	Thickness (mm)		
	2	**3**	**4**
1.Glass	2	3	5
2.Metal	0.5	1	2
3.Wood	2	4	6
4.Insects	2	3	5
5.Hard plastic	2	3	6
6.Soft plastic	2	3	5
7.Rubber	2	3	4
8.Stones	3	4	6

Table 2.1: Thickness of the objects, measured in the direction of which the X-rays transverse through them.

To sum up, three images are available for each of the seven food products, each image contains the 8 foreign objects of the same approximate size. As an example, see Figure 2.8.

(a) Size 4x4x4 mm (b) Size 3x3x3 mm (c) Size 2x2x2 mm

Figure 2.8: Turkey with different sized foreign bodies.

2.3 Methods

In this section, the methods used for preprocessing and feature acquisition will be discussed. In addition, the techniques used for training the classification will also be discussed.

2.3.1 Preprocessing

In real industrial set-ups, the background of the image ought to be removed. Moreover, the characteristics of the packaging and the size and shape of the sliced products will be modelled for each specific industry and product.

The focus of this thesis is not on a single product, so the selected products are imaged without a background or stacking of the product slices. This way, no preprocessing of this kind is necessary.

Nevertheless, some preprocessing needs to be done, which would not be necessary in a conveyor belt solution. Some pixels need to be removed, such as those belonging to the tape used for fixing the samples into the imaging sample container. This is solved with simple masking.

Due to the imaging time constraints, data which only contains food (and no foreign bodies) is not available, so labelling each image into food regions and foreign bodies is necessary. This is used both for training and for validating and testing detection results.

2.3.2 Features

Three spectral features are directly available for every observation/pixel in the image, corresponding to the intensity of the pixel in each of the three modalities. Nevertheless, food and foreign bodies might be easier to separate if more features are added. For this reason, spatial information is also considered, in particular texture features.

2.3.2.1 Texture Features

Texture analysis can be approached in different ways. A focus can be made on the image's first, second or even higher order statistics [Cartensen, 1992], or more complex techniques can be used, such as wavelet features [Arivazhagan and Ganesan, 2003], textons [Leung and Malik, 1999] or Basic Image Features [Crosier and Griffin, 2008].

One of the reasons for the popularity of Basic Image Features is that it allows texture classification without a need for tuning parameters depending on the data set [Crosier and Griffin, 2010]. For this reason, Basic Image Features is the method used for performing texture analysis throughout this thesis.

Basic Image Features (BIF) provide a response vector to seven qualitatively distinct types of local image structure via applying a set of six Gaussian derivative filters to the image at a certain scale σ. Also, the flatness parameter ϵ needs to be set, in order to decide when the surface can be considered to be

uniform (first type of local structure, left of Figure 2.9). The different structures captured by the the BIFs are illustrated in Figure 2.9 [Crosier and Griffin, 2010].

Figure 2.9: Patch stereotypes captured by Basic Image Features (BIF) (Adapted from [Crosier and Griffin, 2010]).

2.3.2.2 Regression/Feature Selection (FS)

The BIF are calculated at three different scales ($\sigma = 1, 5, 10$) and the flatness parameter is fixed to $\epsilon = 0.1$ for simplicity. Consequently, the total number of available features will be

1. Three intensity features, corresponding to the three modalities (absorption, dark-field and phase contrast).
2. Seven texture features per modality and scale, i.e. a total of 63 texture features (7 structures $\times$ 3 scales $\times$ 3 modalities).

For regression and feature selection (FS) purposes there are several methods

1. **Lasso** selects the most relevant features by constraining the $|L|_1$ of the parameters.
2. **Ridge** performs shrinkage by constraining the $|L|_2$ of the parameters.
3. **Elastic net** combines the shrinkage and the parameter selection in order to allow for robust sparse estimates.

The number of observations (pixels) is very high compared to the number of features, so feature selection is not needed. Elastic net needs two parameters to be tuned, so ridge regression is used as it is simpler and more appropriate for this purpose.

Ridge regression minimizes the Euclidean norm between the data and its linear fit, $|L|_2$, while decreasing the negative impact of collinearity between features.

Therefore, it avoids cancellation between correlated features which are relevant for predicting the output when performing Least Square (LS) estimation in a regression context [McDonald, 2009].

2.3.3 Training and Classification Methods

The task of classifying each pixel as belonging to food or to a foreign body requires a trained model. Several methods can be used for classification purposes, two of the simplest, but most appropriate methods, are discussed in this section.

2.3.3.1 GMM

A mixture model is a probabilistic model which represents the presence of one or more populations within an overall population. In particular, a Gaussian mixture model fits a pre-specified number of Gaussians to the data. The number of populations does need to be specified, but there is no need to determine any more information about these populations, other than the observed data. In other words, the learning method is unsupervised. In addition, there can be any number of features/dimensions.

The multivariate ($k = n$ dimensions/features) Gaussian distribution can be written

$$\phi(x|\mu,\Sigma) = \frac{1}{(2\pi)^{n/2}|\Sigma|^{1/2}} \exp^{-1/2(x-\mu)^T\Sigma^{-1}(x-\mu)} \tag{2.1}$$

where μ is the mean vector and Σ is the covariance matrix of the Gaussian distribution. The n-dimensional vector x will be observed in this distribution with a probability ϕ.

The mixture distribution of L Gaussians is

$$p(x) = \sum_{l=1}^{L} p_l \phi(x|\mu_l,\Sigma_l) \tag{2.2}$$

where p_l is the prior probability of each mixture.

In order to fit these Gaussians to the multivariate data, the expectation-maximization (EM) algorithm is used [Dempster et al., 1977]. The Gaussians are initialized to have a random mean and a unitary covariance matrix. The steps expectation (E), which assigns a weight for each cluster, and maximization (M), which calculates the new mean and covariance matrix of the cluster, are performed until the maximum likelihood parameters for the Gaussian model are found, i.e. the best possible fit.

Advantages of using GMM

1. Image noise is typically Gaussian in intensity.
2. Food intensity can be considered as a Gaussian with the mean being water, the food's main constituent part.
3. Only the food needs to be represented in the training set, so any foreign body could be found, even unknown foreign bodies.

Disadvantages of using GMM

1. A number of clusters or sub-populations has to be assumed. This is not an easy task, as the data cannot be visualized when there are more than three features. If this number is not right, the model will be highly inadequate.
2. The probability distribution is specified to be a Gaussian, it is probably close to a Gaussian but the results will not be exact.

The Mahalanobis distance, $D_M(x)$ is the measure which has been chosen in this thesis for calculating the similarity between the image pixels to be classified and the food-fitted Gaussian model.

$$D_M(x) = \sqrt{(x-\mu)^T \Sigma^{-1} (x-\mu)} \tag{2.3}$$

where $x = (x_1, x_2, x_3, ...x_n)^T$ are the feature vectors for each of the N observations/pixels and μ and Σ are the mean vector and covariance matrix of the food model, respectively.

The advantages of the Mahalanobis distance compared to the Euclidean distance is that it is scale-invariant and it considers the correlations within the data set [Bose, 1993].

After calculating the Mahalanobis distance, a hard threshold is set in order to classify each pixel as belonging to food or foreign object.

2.3.3.2 SVM

Support vector machine (SVM) is a supervised learning model. A training data set, which has been previously labelled, is introduced to the SVM training algorithm, which finds a separation between the labelled classes. This separation is optimal if there is no overlapping between these classes. Nevertheless, SVM allows for some misclassification, granting simpler models. This is illustrated in Figure 2.10, where a separation is found, even though some observations are misclassified in Figure 2.10(b). The boundary that separates the classes (food and foreign body) can be chosen to be as simple as a linear function or as complex as wanted by the user, as there is also the possibility of introducing a non pre-specified function [Trevor Hastie, 2008].

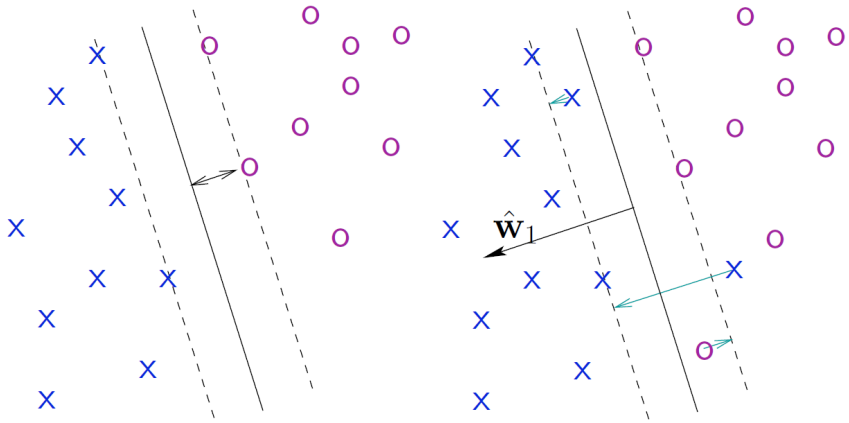

(a) Separable case (b) Non-separable with a linear boundary.

Figure 2.10: Support vector classifiers.

The problem is quadratic with linear inequality constraints, i.e. it is a convex

optimization problem.

$$\begin{aligned} &\underset{\beta\beta_0}{argmin}\frac{1}{2}\|\beta\|^2 + C\sum_{i=1}^{n}\xi_i \\ &\text{subject to } \xi_i \geq 0, y_i(x_i^T\beta + \beta_0) \geq 1 - \xi_i \forall i \end{aligned} \tag{2.4}$$

where the "cost" parameter C is introduced for the non-separable case; the separable case corresponds to $C = \infty$ [Trevor Hastie, 2008]. If it is too large, we have a high penalty for non-separable points and we may store many support vectors and overfit. If it is too small, we may have underfitting [Khan, 2008].

For this particular case-study, a linear boundary will be used for simplicity and overlapping will be allowed to some extent.

As in GMM, there can also be any number of features/dimensions. In fact, as the number of added significant features grows, there is a higher probability of separating the populations correctly.

Advantages of using SVM

1. No assumption is made of probability distribution, so even though food can be approximated by a mixture of Gaussians, the classification could be more accurate if no prior assumption is made about the exact distribution.

Disadvantages of using SVM

1. For this specific case study, the computational time is extremely high because the number of observations is so big. In other cases, this is an advantage of SVM, unlike other methods, it can cope with a large number of features when the number of available observations is not that high.
2. Pixels from every possible class need to be contained in the training data set. As a consequence, foreign bodies of materials which have different properties from those used in the training data set will probably not be found, whereas in GMM any type of foreign body could be found.

Chapter 3

Results

In this section, the focus will be on creating and comparing the different models. For this purpose, only a single food product will be used, namely turkey. Several Gaussian models, with a varying number of features, are fitted to the food observations. These models are optimized, and the pixel-based classification results are compared in order to determine the optimal set of modalities for this specific food product, and whether texture features are worthwhile. After that, the model that performs the best will be compared to the best of the two models that contain only the absorption modality, with and without texture analysis. Then, SVM and GMM's performance are compared for one of the models.

To determine the robustness of the optimal model, three more products are introduced. Will the optimal set of modalities vary from one product to another depending on its absorption, refraction and scattering properties? How good will the model with the optimal set of features and modalities be compared to the optimal absorption model?

3.1 Primary Dataset: Turkey

So as to detect foreign bodies, a model needs to be trained. Next, its parameters need to be optimized and, finally, the model performance needs to be evaluated. Therefore, the total number of observations contained in the three images, corresponding to the three different sized objects, is divided into three sets: training, validation and test set. The food pixels of the training set are used for fitting the food models, the pixels from the validation set are used to tune the parameters of the models and the test set is used to compare the performance of the different models.

3.1.1 Gaussian Models

The following Gaussian models with varying dimensions are subsequently fitted to the food product.

Model nr.	Nr. features	Absorption	Phase contrast	Dark-field	BIF
1	1	Yes	No	No	No
2	1	No	Yes	No	No
3	1	No	No	Yes	No
4	2	Yes	Yes	No	No
5	2	Yes	No	Yes	No
6	2	No	Yes	Yes	No
7	3	Yes	Yes	Yes	No
8	22	Yes	No	No	Yes
9	22	No	Yes	No	Yes
10	22	No	No	Yes	Yes
11	44	Yes	Yes	No	Yes
12	44	Yes	No	Yes	Yes
13	44	No	Yes	Yes	Yes
14	66	Yes	Yes	Yes	Yes

Table 3.1: Different Gaussian models including a varying number of features and imaging modalities.

The parameters that need to be optimized when using Gaussian models are:

1. D, the number of Gaussians which are going to be fitted to the food training data.
2. Th, the hard threshold which is going to be applied to the Mahalanobis distance in order to decide whether a pixel belongs to the food or the foreign body class.

For the seven models with texture features, the Ridge regression parameter k_{ridge} also needs to be specified.

First order statistics, such as the histograms in Figure 3.1, are useful to determine how many Gaussians should be fitted to a certain food product, as they provide an idea of how the data is distributed in intensity. Simple 2D scatter plots, as in Figure 3.2 also provide information on how many Gaussians should be fitted to the data.

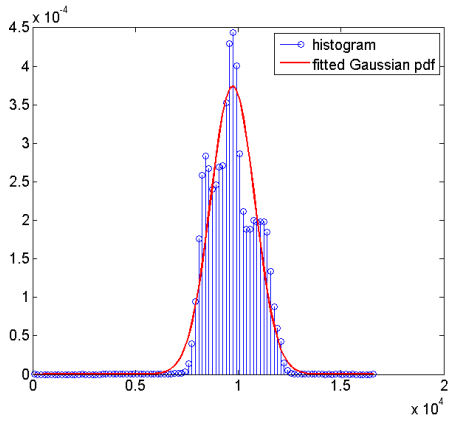

(a) Absorption.

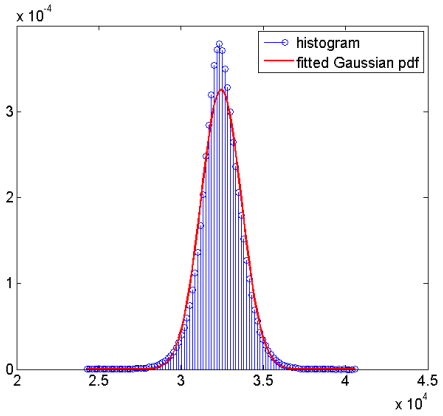

(b) Phase contrast.

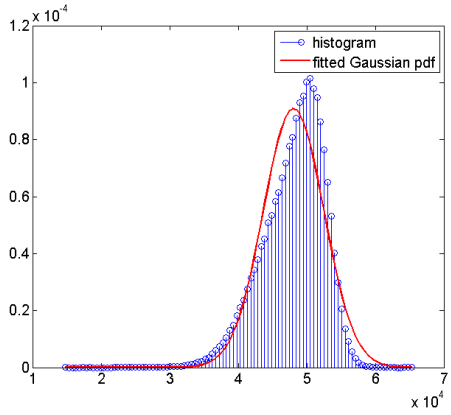

(c) Dark-field.

Figure 3.1: Histograms and fitted Gaussians for turkey intensities in the different modalities.

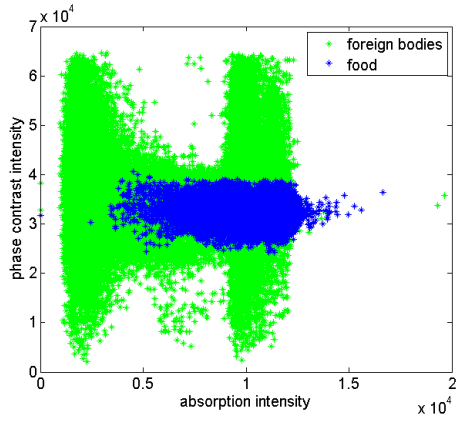

(a) Absorption and phase contrast.

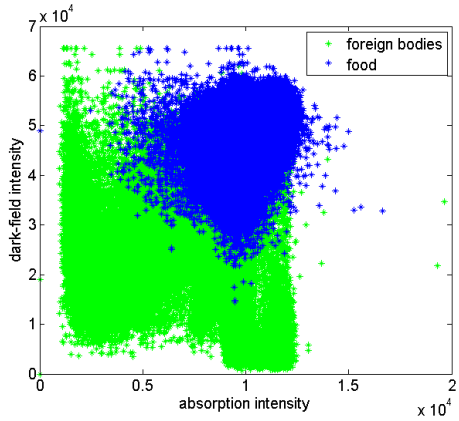

(b) Absorption and dark-field.

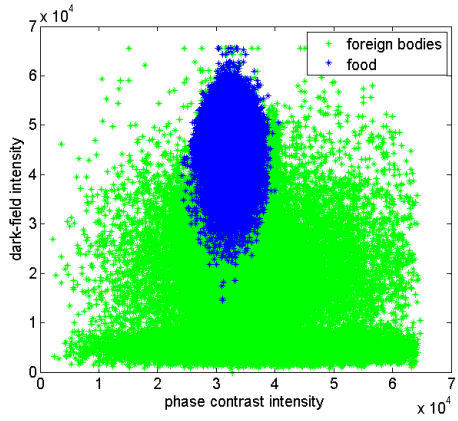

(c) Phase contrast and dark-field.

Figure 3.2: 2D scatter plots for turkey intensities.

By observing Figures 3.1 and 3.2, it is decided to fit one multidimensional Gaussian to the food training data, which means that the parameter D is chosen to be one because the distribution of the intensities seems to follow one single Gaussian. For simplicity, $D = 1$ will be used for each of the fourteen models, even though some of the models include more features, than just the spectral features related to the intensity. Additionally, in Figures 3.1 and 3.2 it can be seen that the food data looks approximately Gaussian, with a higher density of observations towards the middle of the distribution and a lower density as the observations move out from the centre of the distribution.

The parameter k_{ridge} is optimized using the validation set, the optimal k_{ridge} is selected to be the one which minimizes the validation error defined as

$$error = \sqrt{\left(\frac{FN}{N}\right)^2 + \left(\frac{FP}{P}\right)^2} \tag{3.1}$$

where

1. FN is the number of false negative pixels in the validation set, i.e. the number of pixels which are classified as belonging to the false class (food), but are actually from the positive class (foreign bodies).
2. FP is the number of false positives, i.e. the number of pixels that are classified as true (foreign bodies), but actually pertain to the false class (food).
3. N is the number of pixels which actually belong to the negative class, that is to say, the number of food pixels in the validation data.
4. P is the number of pixels that are part of the positive class, the number of foreign body pixels in the validation data.

In Figure 3.3, the validation and training errors are displayed for one of the models, the one including all the possible features.

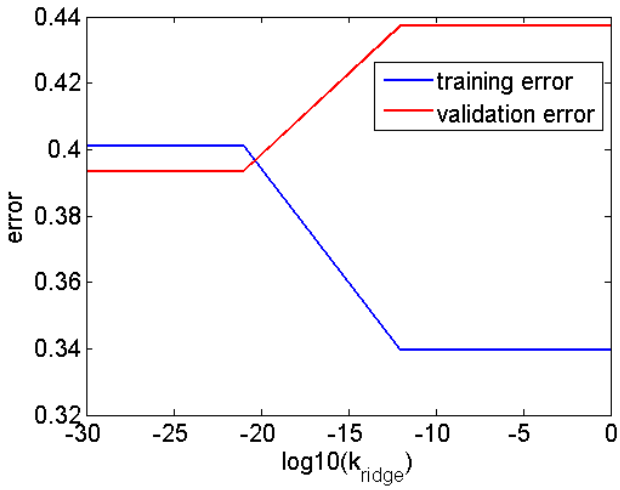

Figure 3.3: Training and validation error for turkey model number 14.

As can be seen in the Figure 3.3, the validation error is not very sensitive to changes in k_{ridge}. This can be better evaluated by looking at the ROC curves. A receiver operating characteristic (ROC curve) illustrates the performance of a two class (binary) classifier and it is created by plotting the sensitivity or true positive rate (TPR) against the 1-specificity or false positive rate (FPR) for varying discrimination thresholds (value from which we decide that a certain pixel belongs to the true class, i.e. that it is a foreign body).

In Figure 3.4, the ROC curves are illustrated for the worst and best value of k_{ridge}, those that correspond to the highest and the smallest validation error, respectively. The euclidean distance, d, from the perfect classifier (TPR=1, FPR=0) to the ROC curve is used to calculate the optimal point of the ROC curve, corresponding to the optimal hard threshold applied to the Mahalanobis distance. In addition, this distance is used to evaluate how well different models perform.

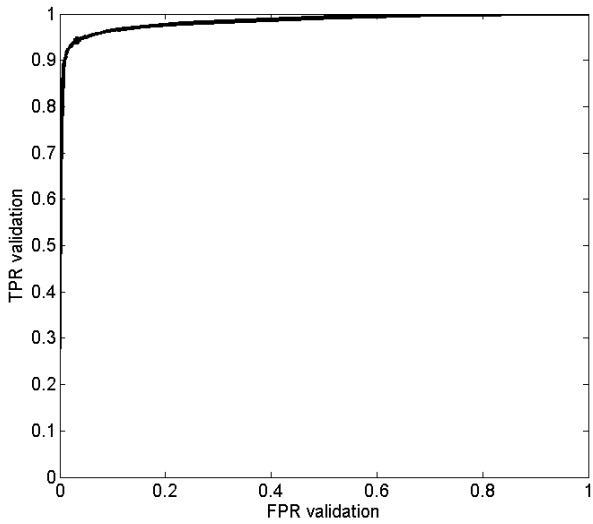

(a) Best case, optimized ($k_{ridge} = 10^{-}21$), $TPR = 0.9437$, $FPR = 0.0337$ and $d = 0.0656$.

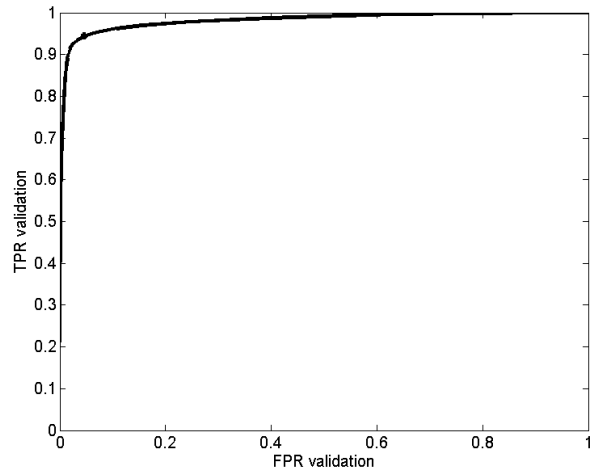

(b) Worst case ($k_{ridge} = 10^{-}12$), $TPR = 0.9447$, $FPR = 0.0468$ and $d = 0.0725$.

Figure 3.4: ROC curves for turkey model 14 with Ridge regression.

The difference between the model with the optimized k_{ridge} and the worst case of k_{ridge} is so small that it is not worthwhile optimizing this parameter, because it takes excessively long. It might not be worthy to use Ridge regression at all. In Figure 3.5, the ROC curve is represented for the turkey model number 14, but without including Ridge regression.

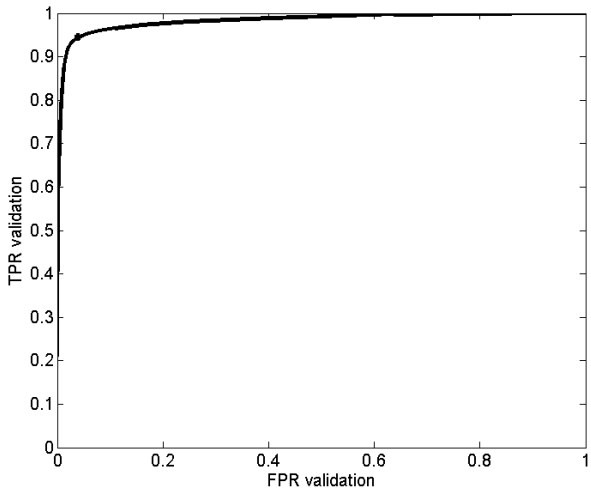

Figure 3.5: ROC curve for turkey model 14 without Ridge regression. $TPR = 0.9448$, $FPR = 0.0393$ and $d = 0.0678$.

From Figure 3.5 it can be inferred that Ridge regression does not add significant benefits, as the distance from the optimized threshold to the ideal classifier is 0.0656 when using Ridge, compared to 0.0678 when Ridge is not used. These distances are very similar, so Ridge regression will not be used from here onwards so as to avoid a time-consuming optimization study.

In Figure 3.6, the thresholds have been optimized for each of the 14 food models, the optimal points are the closest points from each ROC curve to the ideal classifier (TPR=1, FPR=0), and are marked in the graphs.

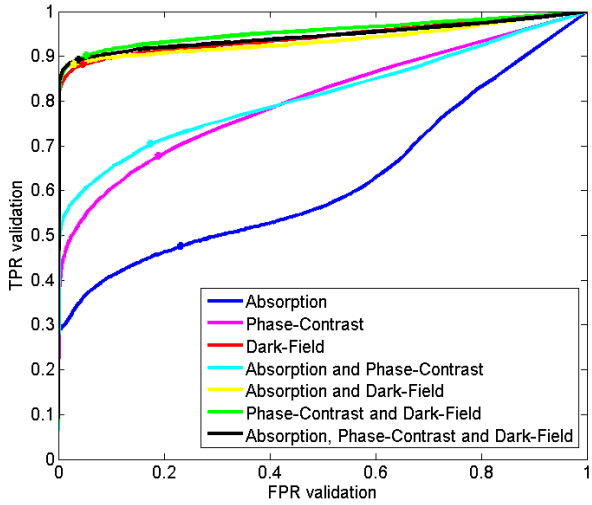

(a) Turkey models without BIF features.

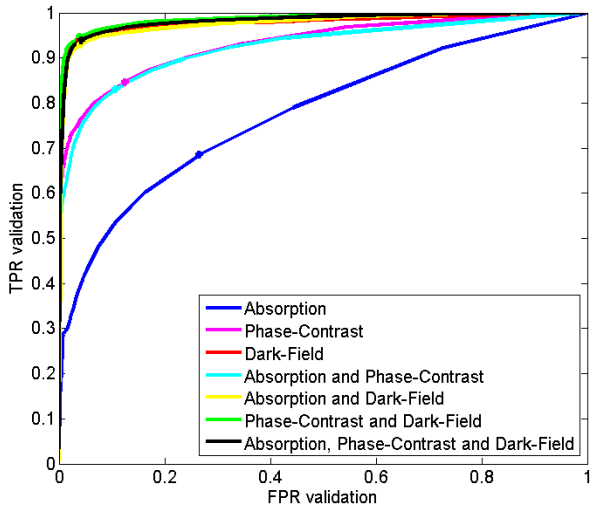

(b) Turkey models including BIF features.

Figure 3.6: ROC curves for turkey models.

By looking at the ROC curves, the qualitative performance of each model can be assessed. However, to present the quantitative performance of the different models, the distances from each of the optimal 14 models to the ideal classifier are displayed in the following Table, starting with the best performance model to the worst performance model (pixel-wise classification).

Distance d	Model Nr.
0.0664	13
0.0720	10
0.0739	14
0.0811	12
0.1113	6
0.1135	7
0.1205	5
0.1260	3
0.1976	9
0.2003	11
0.3437	4
0.3741	2
0.4116	8
0.5723	1

Table 3.2: Distances from the optimized turkey models to the ideal classifier.

Improved performance of the models is observed when texture analysis is included, so it is advantageous to add these extra spatial features. Moreover, the optimal model for turkey is the one which includes the phase contrast and dark-field modalities, and the worst model is the one that only contains the absorption intensity.

However, the performance of the models should be measured using the set of observations/pixels that belong to the test set. In Table 3.3 the confusion matrix (CM) is displayed for the model number 13 and for the absorption model which performs best, number 8, as well as the values for the precision and accuracy measures. These measures a defined as follows

$$precision = TP/P \tag{3.2}$$

$$accuracy = \frac{TP + TN}{P + N} \tag{3.3}$$

Model nr.	Nr. feat.	TP	FP	TN	FN	Precision	Accuracy
13	44	3569	1211	38806	225	0.9407	0.9672
8	22	2624	10183	29834	1170	0.6916	0.7409

Table 3.3: Turkey models performance on test set.

In Figure 3.7, the distance maps can be observed for two models. First, the turkey model which performs the best out of the two models that only include the absorption modality information, i.e. the best classifier out of the models number 1 and 8. Second, the turkey model that performs best out of the 14 models. In Figure 3.8, the corresponding final classification decisions for each pixel are portrayed.

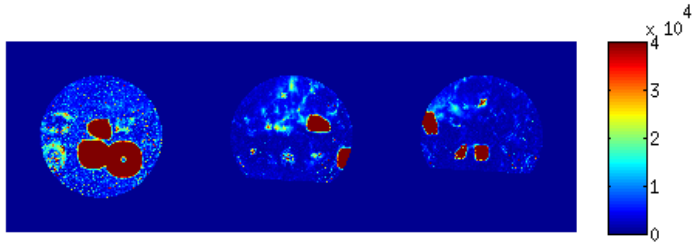

(a) Best absorption turkey model, model number 8.

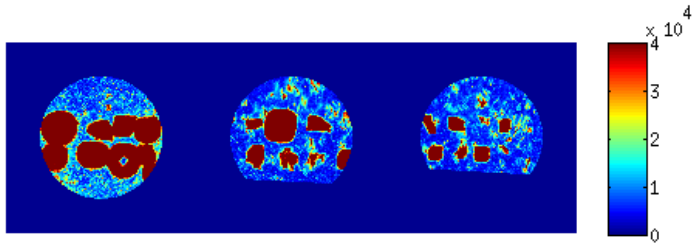

(b) Best turkey model, model number 13.

Figure 3.7: Distance maps.

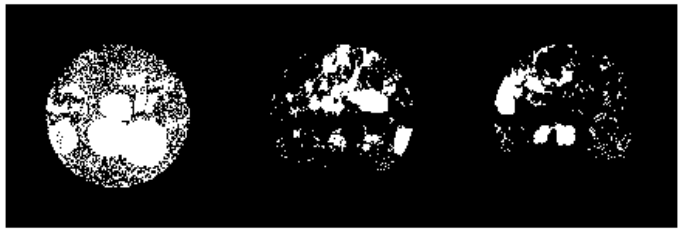

(a) Best absorption turkey model, model number 8.

(b) Best turkey model, model number 13.

Figure 3.8: Thresholded images, final classification.

3.1.2 Gaussian Model VS Support Vector Machine

As in GMM, the data set is divided into training, validation and test set. In contrast to GMM, not only the food pixels, but also the foreign bodies, are represented in the training set.

The performance of the Gaussian model is going to be compared to the performance of SVM for the turkey model number 10, the one which includes the dark-field modality, with its spectral and texture features.

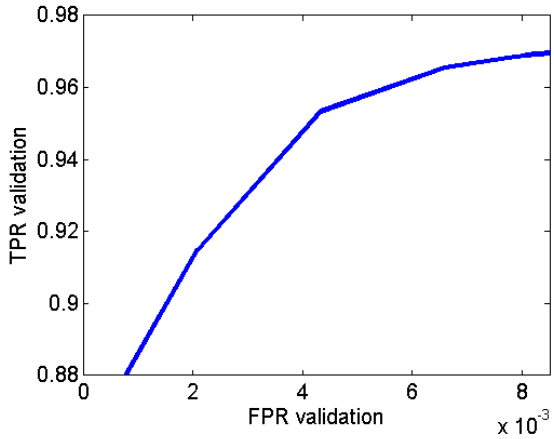

(a) Turkey SVM model, $d = 0.0468$.

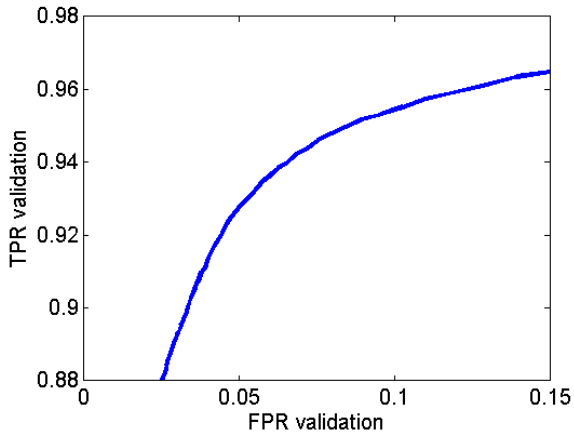

(b) Turkey GMM model, $d = 0.0712$.

Figure 3.9: ROCs for turkey dark-field models, including texture features.

SVM's performance is better, as can be perceived qualitatively from Figure 3.9 and quantitatively from the distance d values ($d = 0.0468$ for SVM and $d = 0.0712$ for GMM), but it has to be taken into account that Support Vector Machines performance will rapidly decrease when the foreign bodies in the test set differ from those represented in the training set. Moreover, another reason for choosing GMM against SVM, is that the latter takes much longer to be trained.

3.2 Extended Dataset: Cheese, Salami and Rye Bread.

The next three products will be analysed using Gaussian Models and no Ridge regression, because of the reasons stated above.

The following results are obtained for cheese (Figure 3.10), salami (Figure 3.11) and rye bread (Figure 3.12). Thanks to the ROC curves, the performance of the different models can be compared visually.

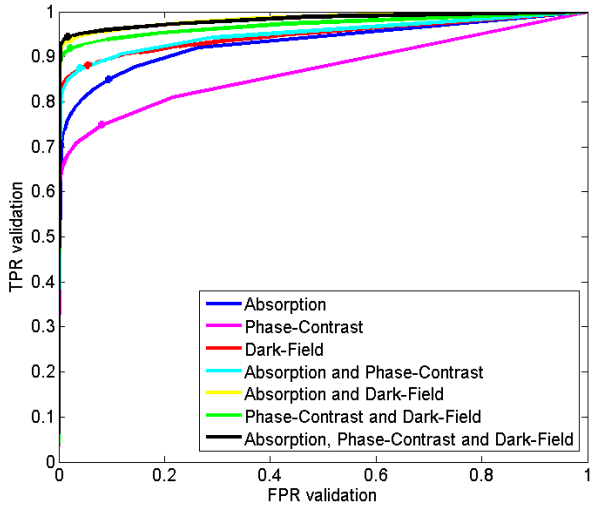

(a) Cheese models without BIF features.

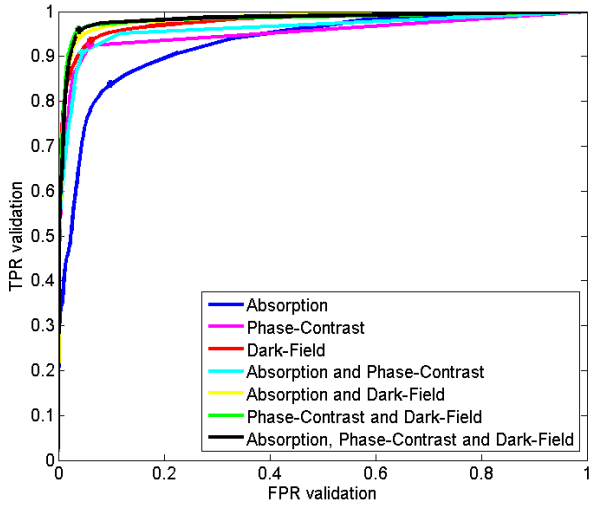

(b) Cheese models including BIF features.

Figure 3.10: ROCs for cheese models.

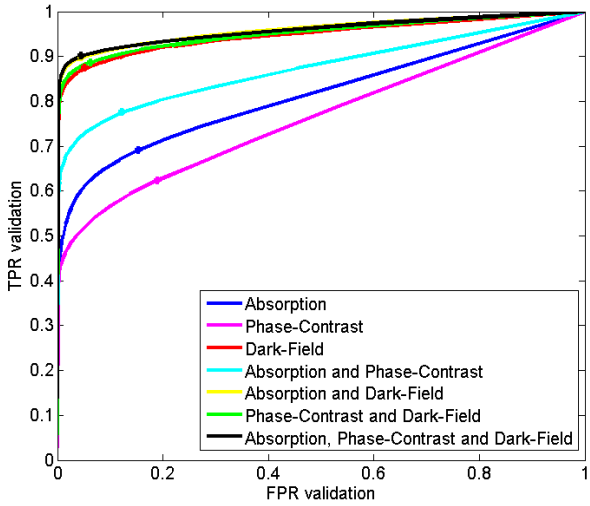

(a) Salami models without BIF features.

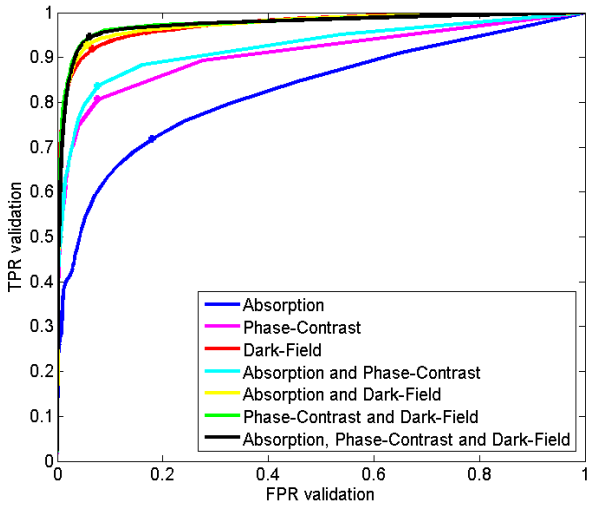

(b) Salami models including BIF features.

Figure 3.11: ROCs for salami models.

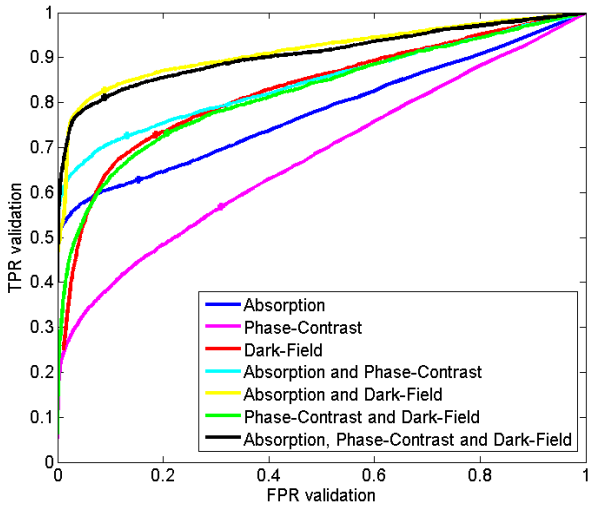

(a) Rye bread models without BIF features.

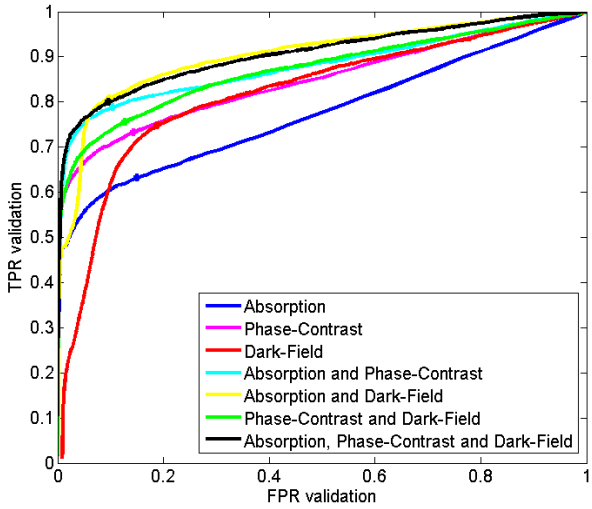

(b) Rye bread models including BIF features.

Figure 3.12: ROCs for rye bread models.

The performance of the different models can be assessed quantitatively by comparing the euclidean distance d from the optimal point for each model to the ideal classifier. These distances are displayed in Table 3.4 for cheese, salami and rye bread.

Cheese		**Salami**		**Rye bread**	
Model nr.	d	**Model nr.**	d	**Model nr.**	d
13	0.0563	13	0.0814	5	0.1936
14	0.0576	14	0.0820	7	0.2081
7	0.0632	12	0.0915	12	0.2146
12	0.0668	10	0.1054	14	0.2215
5	0.0678	7	0.1083	11	0.2353
6	0.0854	5	0.1119	13	0.2747
10	0.0892	6	0.1286	9	0.3026
9	0.0978	3	0.1362	4	0.3037
11	0.1021	11	0.1801	10	0.3143
3	0.1271	9	0.2078	3	0.3282
4	0.1381	4	0.2551	6	0.3388
1	0.1794	8	0.3335	8	0.3969
8	0.1882	1	0.3445	1	0.4011
2	0.2694	2	0.4209	2	0.5304

Table 3.4: Distances from the optimized models to the ideal classifier.

Note how the different models perform on different food products. Model 13 outperforms the others for cheese and salami, however does not perform so well on rye bread, where model 5 gives the best results.

Moreover, improved detection is observed when Basic Image Features are added to the model, except for rye bread models, where BIF features do not add significant benefit.

In fact, the detection rate is quite poor for rye bread, this could be due to the fact that the seeds it contains look like foreign bodies. In order to add BIFs for rye bread, an extensive optimization study on the scales and measure of flatness used for the smoothing should be performed. Perhaps better results can be obtained when these have been optimized. Nevertheless, including the dark-field and phase-contrast modalities does improve the detection of foreign bodies in rye bread.

In Table 3.5 the performance of the models on the test set can be compared.

Product	Model	Nr. feat.	TP	FP	TN	FN	Prec.	Acc.
Cheese	13	44	7984	1268	32604	352	0.9578	0.9616
	1	1	7129	3494	30379	1189	0.8571	0.8890
Salami	13	44	6834	2125	37484	449	0.9383	0.9451
	8	22	5491	8682	30917	1803	0.7528	0.7764
Rye Bread	12	44	2319	4582	43245	541	0.8108	0.8989
	8	22	1787	6934	40910	1056	0.6286	0.8424

Table 3.5: Models performance on test set.

Finally, the resulting pixel-based classification can be compared for the best of the two available absorption models against the model which performs the best out of the 14 models. This provides a visual representation of the gain obtained by adding these new imaging modalities: phase contrast and dark-field.

In Figures 3.13, 3.15 and 3.17 the distance maps can be observed for the model that performs best for each food product compared to the product's absorption model out of the two absorption models, number 1 and 8, which provides the better classification. In Figure 3.14, 3.16 and 3.18 the corresponding final classification decisions for each pixel are portrayed.

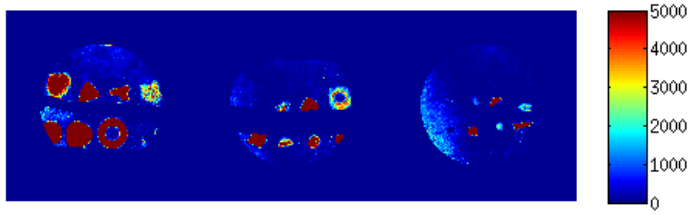

(a) Best absorption cheese model, model number 1.

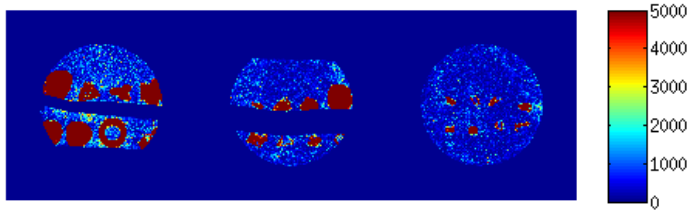

(b) Best cheese model, model number 13.

Figure 3.13: Distance maps.

(a) Best absorption cheese model, model number 1.

(b) Best cheese model, model number 13.

Figure 3.14: Thresholded images, final classification.

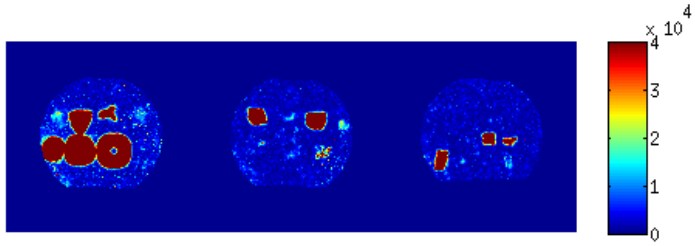

(a) Best absorption salami model, model number 8.

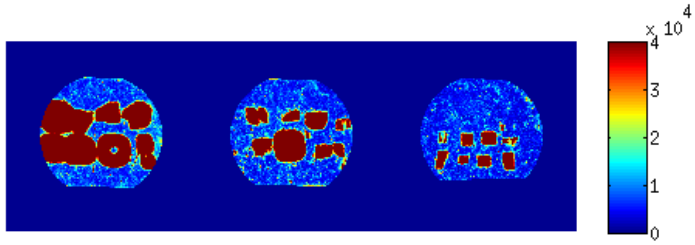

(b) Best salami model, model number 13.

Figure 3.15: Distance maps.

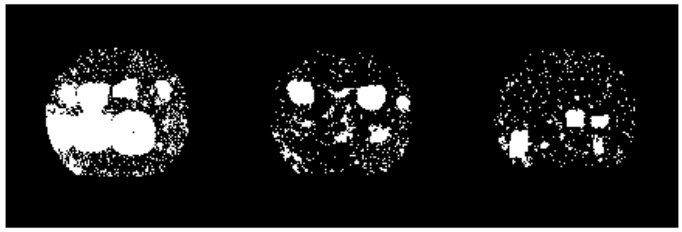

(a) Best absorption salami model, model number 8.

(b) Best salami model, model number 13.

Figure 3.16: Thresholded images, final classification.

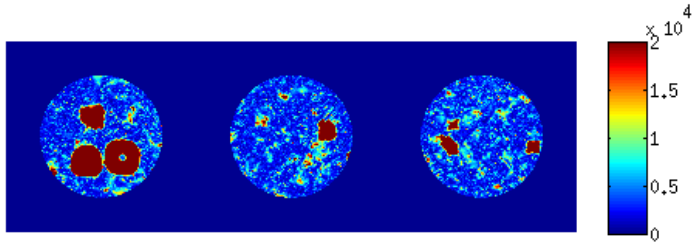

(a) Best absorption rye bread model, model number 8.

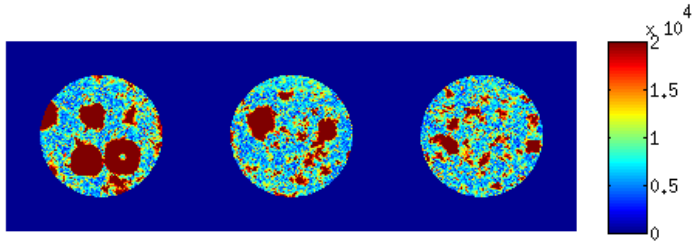

(b) Best rye bread model, model number 12.

Figure 3.17: Distance maps.

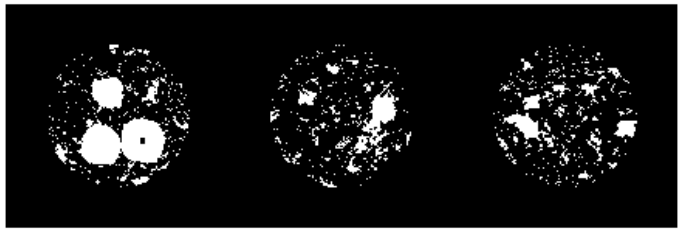

(a) Best absorption rye bread model, model number 8.

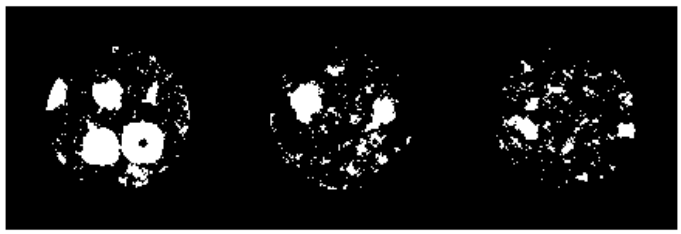

(b) Best rye bread model, model number 12.

Figure 3.18: Thresholded images, final classification.

Chapter 4

Conclusions and future work

The most important result of this thesis is the fact that it gives evidence towards an improved and efficient automatic foreign body detection when adding two additional imaging modalities (phase contrast and dark-field) to the well-known absorption contrast modality. These two modalities enable the detection of organic matter, which is very difficult to find with conventional X-rays.

Dark-field is the modality where organic foreign bodies best show up, also non-organic foreign bodies can be seen in this modality, so absorption does not add that much information once the dark-field modality is available. Nevertheless, phase contrast and absorption modalities can add to the model some extra information that the dark-field modality does not capture. For cheese, the absorption modality adds more information than the phase contrast modality, whereas for the other three products, the models that include phase contrast perform better than those that include the absorption modality. If no texture features have been added, models that include only the absorption modality usually perform better than those including only the phase contrast modality. Regarding texture analysis, the calculation of the BIFs is worthwhile as an improved detection is observed when these features are added to the model. However, if the texture of the food product is complex, such as rye bread's texture, then an extensive study should be performed in order to select the parameters that give the most information.

It should be pointed out that, although constructing the food models is time consuming, the classification of new data is easy because only the BIF features and the Mahalanobis distance (or the SVM result) need to be calculated. These calculations are fast and mainly pixel-wise operations (apart from the BIFs). Therefore, they can be easily parallelized and implemented to run fast on, for example, a GPU. This is very important when considering a conveyor belt solution.

SVM will not perform adequately if 'new' foreign bodies (different from those in the training set) appear in the food products. It is not possible to create a perfect training set, one which represents all possible foreign bodies, so future work should focus on GMM.

The number of Gaussians, D, was chosen by just looking at the intensity features. However, this parameter could be optimized by splitting the data in more than one validation set, as there are many more features than just intensity features. Moreover, object-based detection should be performed for a more robust classification, as well as to provide an estimation of the sizes that could be detected.

What is more, the models could be tested with unseen data, such as bones or other foreign bodies which have not been included in the development of the models. Actually, a test set of this nature, which contains foreign bodies which have not been used for training nor tuning these models, was also acquired at TUM.

Ridge does not introduce gain in this specific case study, but more complex models could be created with a higher number of spatial features in order to analyse complex textures, such as rye bread's texture. By adding more flatness parameters and more scales to the texture analysis, the dimensionality quickly increases. Then, elastic net could be probed to eliminate irrelevant scales and/or flatness parameters in order to decrease the computational time of the BIF features because, due to speed restrictions, BIF features cannot be calculated for a high number of scales and flatness parameters in a conveyor belt solution.

All in all, grating-based interferometry (GBI) allows detection of organic matter and performs much better than typical X-ray when there is a mix of organic and non-organic foreign bodies. As a consequence, a quality assurance conveyor belt solution with GBI would be much more efficient than one with typical X-rays for industries where organic materials are potential foreign bodies.

Appendix A

Data set

A.1 Turkey

In Figures A.1, A.2 and A.3 the three images for turkey, corresponding to the three different sized foreign bodies can be observed. Each image consists of three modalities with pixel correspondence: absorption, phase contrast and dark-field.

(a) Absorption (b) Phase contrast (c) Dark-field

Figure A.1: Turkey containing foreign bodies of approximately 2x2x2 mm.

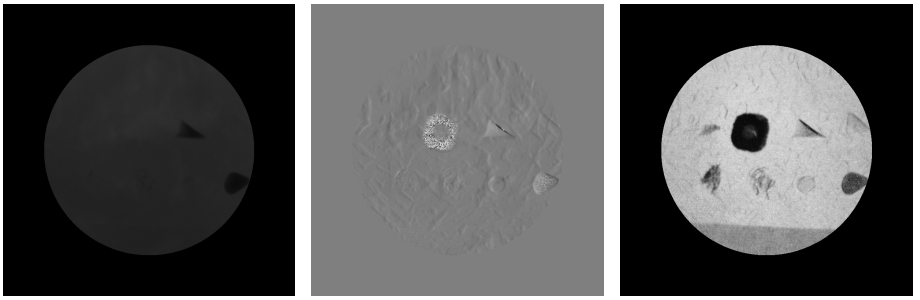

(a) Absorption (b) Phase contrast (c) Dark-field

Figure A.2: Turkey containing foreign bodies of approximately 3x3x3 mm.

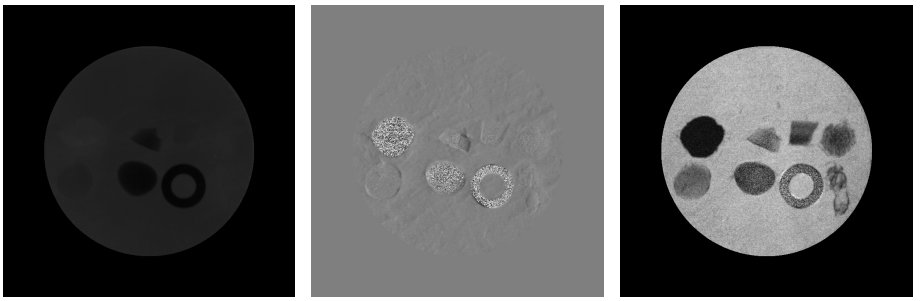

(a) Absorption (b) Phase contrast (c) Dark-field

Figure A.3: Turkey containing foreign bodies of approximately 4x4x4 mm.

A.2 Cheese

In Figures A.4, A.5 and A.6 the three images for cheese, corresponding to the three different sized foreign bodies can be observed. Each image consists of three modalities with pixel correspondence: absorption, phase contrast and dark-field.

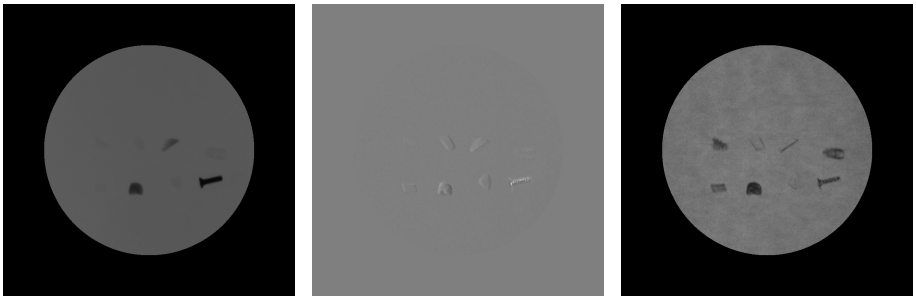

(a) Absorption (b) Phase contrast (c) Dark-field

Figure A.4: Cheese containing foreign bodies of approximately 2x2x2 mm.

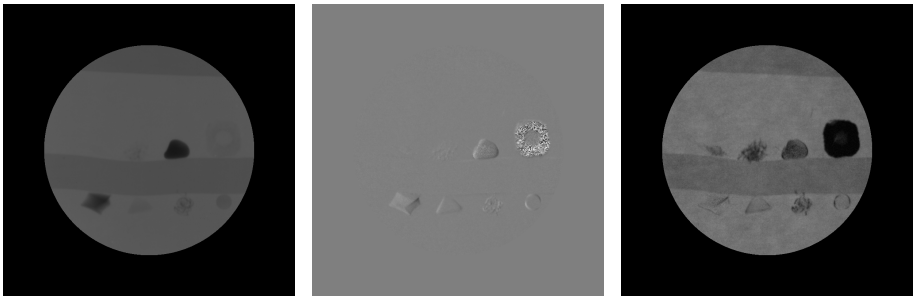

(a) Absorption (b) Phase contrast (c) Dark-field

Figure A.5: Cheese containing foreign bodies of approximately 3x3x3 mm.

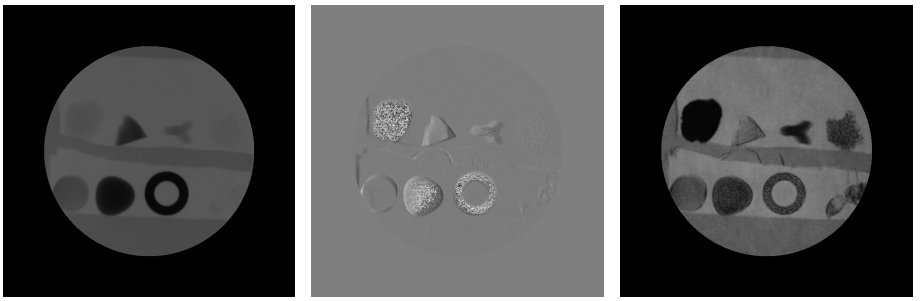

(a) Absorption (b) Phase contrast (c) Dark-field

Figure A.6: Cheese containing foreign bodies of approximately 4x4x4 mm.

A.3 Salami

In Figures A.7, A.8 and A.9 the three images for salami, corresponding to the three different sized foreign bodies can be observed. Each image consists of three modalities with pixel correspondence: absorption, phase contrast and dark-field.

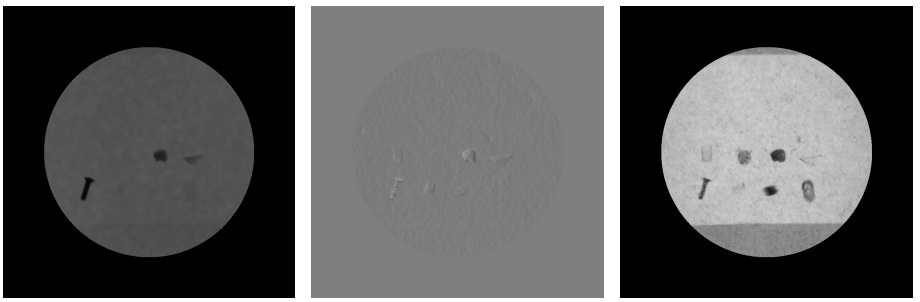

(a) Absorption (b) Phase contrast (c) Dark-field

Figure A.7: Salami containing foreign bodies of approximately 2x2x2 mm.

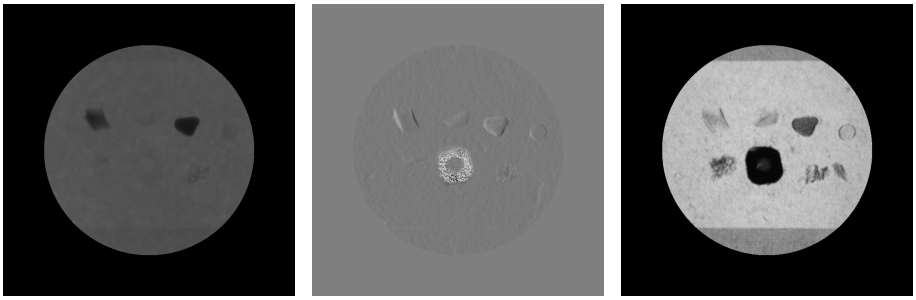

(a) Absorption (b) Phase contrast (c) Dark-field

Figure A.8: Salami containing foreign bodies of approximately 3x3x3 mm.

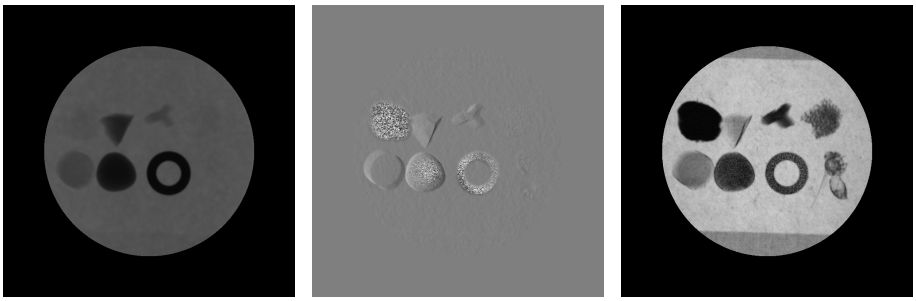

(a) Absorption (b) Phase contrast (c) Dark-field

Figure A.9: Salami containing foreign bodies of approximately 4x4x4 mm.

A.4 Rye bread

In Figures A.10, A.11 and A.12 the three images for rye bread, corresponding to the three different sized foreign bodies can be observed. Each image consists of three modalities with pixel correspondence: absorption, phase contrast and dark-field.

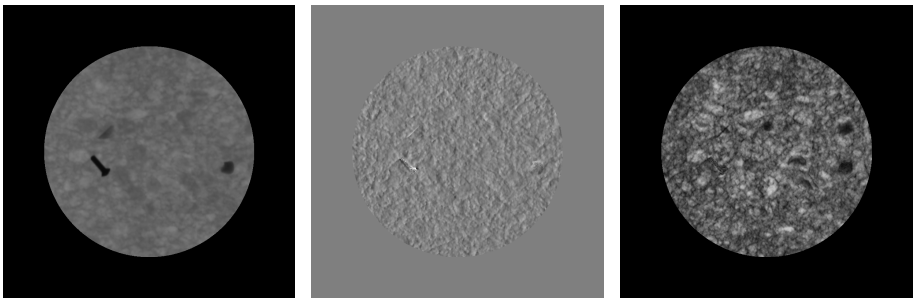

(a) Absorption (b) Phase contrast (c) Dark-field

Figure A.10: Rye bread containing foreign bodies of approximately 2x2x2 mm

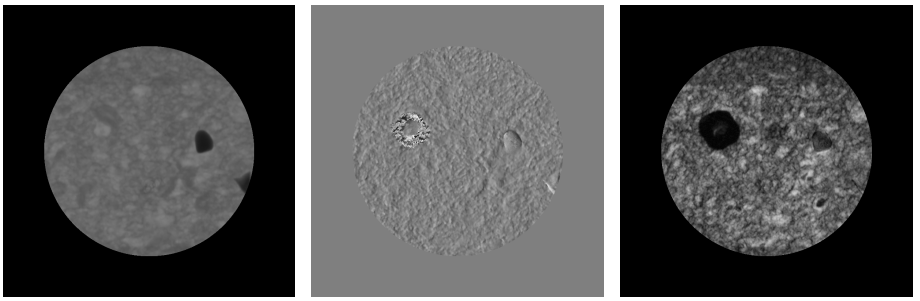

(a) Absorption (b) Phase contrast (c) Dark-field

Figure A.11: Rye bread containing foreign bodies of approximately 3x3x3 mm

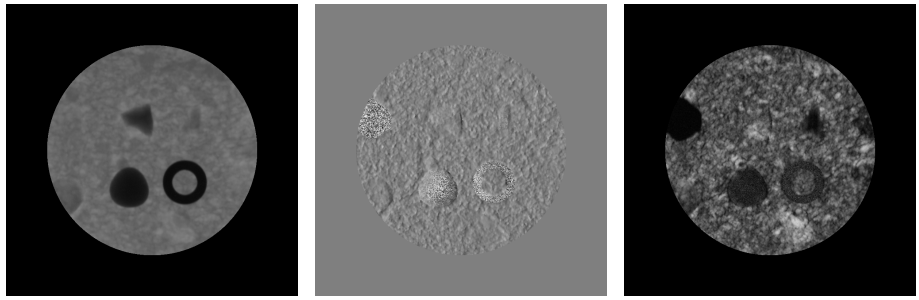

(a) Absorption (b) Phase contrast (c) Dark-field

Figure A.12: Rye bread containing foreign bodies of approximately 4x4x4 mm

Bibliography

[Arivazhagan and Ganesan, 2003] Arivazhagan, S. and Ganesan, L. (2003). Texture classification using wavelet transform. *Pattern recognition letters*, 24(9-10):1513–1521.

[B. G. Batchelor and Graves, 2004] B. G. Batchelor, E. R. D. and Graves, M. (2004). Using x-rays to detect foreign bodies. In Edwards, M., editor, *Detecting foreign objects in food*, pages 226–264. Woodhead Publishing Ltd.

[Bech, 2009] Bech, M. (2009). *X-ray imaging with a grating interferometer*. PhD thesis, University of Copenhagen, Niels Bohr Institute.

[Bose, 1993] Bose, S. (1993). Mahalanobis, prasanta, chandra. *Current Science*, 65(1):96–97.

[Cartensen, 1992] Cartensen, J. M. (1992). *Description and simulation of visual texture, chapter 1.* PhD thesis, Technical University of Denmark, Department of Informatics and Mathematical Modeling.

[Crosier and Griffin, 2008] Crosier, M. and Griffin, L. (2008). Texture classification with a dictionary of basic image features. *IEEE Conference on Computer Vision and Pattern Recognition (CVPR)*, pages 1–7.

[Crosier and Griffin, 2010] Crosier, M. and Griffin, L. (2010). Using basic image features for texture classification. *International Journal of Computer Vision*, 88(3):447–460.

[Dempster et al., 1977] Dempster, A., Laird, N., and Rubin, D. (1977). Maximum likelihood from incomplete data via em algorithm. *Journal of the Royal statistical society series b-methological*, 39(1):1–38.

[F. Pfeiffer and David, 2006] F. Pfeiffer, T. Weitkamp, O. B. and David, C. (2006). X-ray dark-field imaging for detection of foreign bodies in food. *Nature Physics*, 2.

[Hooke, 1665] Hooke, R. (1665). *Micrographia*. Royal Society.

[Khan, 2008] Khan, S. (2008). Ethem alpaydin. introduction to machine learning (adaptive computation and machine learning series). *Natural Language Engineering*, 14.

[Kottler et al., 2010] Kottler, C., Revol, V., Kaufmann, R., Urban, C., Knop, K., Sennhauser, U., Jerjen, I., Luthi, T., Cardot, F., and Niedermann, P. (2010). Phase sensitive x-ray imaging: Towards its interdisciplinary applications. *AIP conference proceedings*, 1236:213–218.

[Leung and Malik, 1999] Leung, T. and Malik, J. (1999). Recognizing surfaces using three-dimensional textons. 2:1010–1017 vol.2.

[M. S. Nielsen and Fidenhans, 2012] M. S. Nielsen, T. Lauridsen, L. B. C. and Fidenhans, R. (2012). X-ray dark-field imaging for detection of foreign bodies in food. *Elsevier*.

[McDonald, 2009] McDonald, G. C. (2009). Ridge regression. *Wiley Interdisciplinary Reviews: Computational Statistics*, 1(1):93–100.

[Nielsen, 2012] Nielsen, M. S. (2012). Novel x-ray imaging modalities - seeing through food. Master's thesis, University of Copenhagen, Niels Bohr Institute.

[Röntgen, 1895] Röntgen, W. C. (1895). Über eine neue art von strahlen. In *Sitzungsberichte der Physikalisch-Medizinischen Gesellschaft in Würzburgt*, volume 137, pages 132–141.

[Rost and Oldfield, 2000] Rost, F. W. D. and Oldfield, R. J. (2000). *Photography with a microscope*. Cambridge University Press.

[Scherer et al., 2014] Scherer, K., Birnbacher, L., Chabior, M., Herzen, J., Mayr, D., Grandl, S., Sztrókay-Gaul, A., Hellerhoff, K., Bamberg, F., and Pfeiffer, F. (2014). Bi-directional x-ray phase-contrast mammography. *PloS One*, 9(5):e93502.

[Spiegel, 1995] Spiegel, P. K. (1995). The first clinical x-ray made in america-100 years. In *AJR Am J Roentgenol*, volume 164, pages 241–243.

[Takashi, 2009] Takashi, A. (2009). Detection for foreign bodies and bones in meat and meat products. In *International Congress of Meat Science and Technology*, 55, Copenhagen, Denmark.

[Trevor Hastie, 2008] Trevor Hastie, Robert Tibshirani, J. F. (2008). Support vector machines and flexible discriminants. In *The Elements of Statistical Learning: Data Mining, Inference, and Prediction. 2nd edition.* Springer.

[Zernike, 1942] Zernike, F. (1942). Phase contrast, a new method for the microscopic observation of transparent objects part ii. In *Physica*, volume 9, pages 974–986.